Model predictive control for a university heat prosumer with data centre waste heat and thermal energy storage

Juan Hou[a*], Haoran Li[a], Natasa Nord[a], Gongsheng Huang[b]

[a]Department of Energy and Process Technology, Norwegian University of Science and Technology, Kolbjørn Hejes vei 1 B, Trondheim 7491, Norway

[b]Department of Architecture and Civil Engineering, City University of Hong Kong, Y6621, AC1, Tat Chee Ave, Kowloon, Hong Kong

*Corresponding author, Email: juan.hou@ntnu.no

Abstract

Data centres (DCs) are energy-intensive facilities that convert most of their energy use into waste heat. Given the rapidly increasing energy and environmental impacts of DCs, and the need to optimize regional energy structures, there is an increasing effort to recover DC waste heat for district heating (DH) systems. However, previous research mainly focused on exploring the possibilities and proposing technical solutions for capturing DC waste heat for DH systems. They rarely investigated solutions on optimal control of the DH system after recovering DC waste heat, particularly for a DC waste heat-based heat prosumer with thermal energy storage (TES). Therefore, this study applied a model predictive control (MPC) scheme for a university heat prosumer with DC waste heat and water tank TES by simulation. In the framework, the objective function minimized the overall energy cost considering the dynamic heating and electricity prices simultaneously, and the incorporated model described system dynamics including DC waste heat recovery units, TES, and campus DH system. The MPC framework was demonstrated to be more effective than a traditional rule-based control approach in terms of 1) providing more stable chilled water for the DC cooling system and 2) cutting monthly energy costs by up to 3.2%.

Keywords: district heating system, distributed heat source, optimal control, economic boundary, energy cost.

Nomenclature

COP	Coefficient of performance
CP	Circulator pump
DC	Data centre
DH	District heating
DHS	Distributed heat source
EDC	Energy demand component
HE	Heat exchanger
HP	Heat pump
IT	Information technology
LDC	Load demand component
MAE	Mean absolute error
MAPE	Mean absolute percentage error
MPC	Model predictive control
MS	Main substation
NLP	Nonlinear programming
PI	Proportional-integral
RBC	Rule-based control
RMSE	Root mean square error
TES	Thermal energy storage
WCC	Weather compensation controller
WTTES	Water tank thermal energy storage

1. Introduction

District heating (DH) systems, which satisfy buildings' heat demand in an energy-efficient and environment-friendly way, has been globally used for more than a century. Nowadays, the total number of DH systems has been estimated to be around eighty thousand all overall the world, thereof about six thousand systems in Europe [1, 2]. However, with the transition from current energy systems to future sustainable energy solutions, the DH system, as an essential part of the energy systems, must undergo a generational transition to maintain its competitiveness compared with

alternative heating technologies [3]. As a result, the current second and third-generation DH systems are evolving towards the fourth and fifth-generation DH systems. Integrating renewables and waste heat into the DH system is one significant characteristic of the future DH system [3, 4]. Specifically, the renewables and waste heat can be integrated into the heat user side as distributed heat sources (DHSs), and these heat users with DHSs are known as heat prosumers because of their dual roles as producers and consumers [5]. In the future, heat prosumers will become critical participants in DH systems due to the increasing integration of renewables and waste heat [6]. In general, a large number of renewables and waste heat, such as solar thermal energy, geothermal energy, data centre (DC) waste heat and industrial waste heat, are available for heating purposes in most parts of the world. Among these, the waste heat from a DC is a promising heat source because of its evenly distributed load profile and waste heat generation [7, 8]. In addition, many DCs are constructed close to an existing DH network, which makes the DC waste heat is easy to access for the DH network.

The integration of DC waste heat with the DH system is beneficial for the energy efficiency improvement of DCs as well. The rapid growth of the need for data processing, storage, and digital telecommunications has led to a dramatic increase in the DC industry [9]. A DC houses information technology (IT) equipment for data processing and storage, as well as communications networking. Moreover, a DC typically includes environmental control equipment to ensure the proper working environment of IT equipment. These two major energy end-user equipment results in a DC an energy-intensive facility. A DC can be more than 40 times as energy-intensive as a conventional office building [10]. Therefore, with the concerns of energy and climate crisis, exploring the techniques for energy efficiency improvements of DCs is imperative[9]. Capturing and reusing the DC waste heat for a DH system is an effective way to improve the DC's energy efficiency, especially in Nordic countries. Firstly, the cold climate in Nordic countries is ideal for DCs, since it provides much-needed cooling energy for DCs. Meanwhile, these countries have a significant demand for heat [7]. Secondly, a large portion of the electricity used in DCs is converted into waste heat. For a typical DC, approximately half of the electricity used ultimately becomes waste heat [11, 12].

Due to the merits explained above, there is a growing effort to integrate DCs' waste heat into DH systems and consequently contribute to the sustainability of the energy systems. Li et al. evaluated the financial benefit of recovering DC waste heat for a DH system by a CO_2 heat pump (HP). Results showed that the DC waste heat heating system could reduce the annual energy cost by 23-75% compared with other common heating methods [13]. Wahlroos et al. analysed DC waste heat

utilization for a DH system. Simulated results showed that with high shares of DC waste heat in the investigated DH system, the annual operational cost savings were 0.6–7.3% [7]. Hiltunen et al. evaluated the possibility of utilizing DC waste heat for the DH system in the city of Espoo, Finland to realize the decarbonisation goal in the near future. Simulation results showed that the integration of DC waste heat with the DH system enabled CO_2 emissions reduction yet prevented the increase of production costs [14]. Davies et al. investigated the potential of utilizing DC waste heat for the DH system in London and calculated the possible savings of waste heat reuse in a DH system. Results showed that nearly £ 1 million in energy cost was saved per year for the case of a 3.5 MW DC [15]. He et al. proposed a distributed cooling solution to capture the waste heat from a DC for a DH system, and the proposed method was implemented in a DC in Hohhot, China. Results showed that the proposed waste heat utilization technology saved around 18 thousand tons of standard coal each year compared to the coal-fired boiler heating system [16]. Furthermore, Wahlroos et al. analysed the potential for reusing DC waste heat in DH systems, and presented an overview of several successful DC waste heat utilization projects, especially in Nordic countries [17].

These previous studies have demonstrated the enormous economic benefits of integrating DC waste heat with the DH network. However, these studies are mainly subject to exploring the possibilities and proposing technical solutions for capturing DC waste heat for DH systems. The research focusing on the optimal control of the DH system after integrating DC waste heat is hardly found, especially for the optimal control of a DC waste heat-based heat prosumer. An optimal control strategy may fully unlock the flexibilities of the system and further improve the economic performance of the DH system. However, the optimal control of a DC waste heat-based heat prosumer is challenging, and the difficulties come from the following aspects: 1) a complex economic boundary involving not only dynamic heating prices but also electricity prices due to the electricity use of DC waste heat recovery units, 2) multi-level technical operation constraints from both the DH system and the cooling system of the DC, and 3) numerous manipulated variables need to be optimized originating from the multi-components, such as heat substation, heat users, or DC. Moreover, introducing thermal energy storage (TES), which is widely used to perform peak load shaving in DH systems, to the DC waste heat-based heat prosumer would further increase the complexity of the system as well as the complexity of the optimal control.

Model predictive control (MPC), which can employ an economic-related objective function for real-time control, is an ideal optimal control strategy to realize the maximized possible economic

performance of the system while satisfying different technical operational constraints [18, 19]. In addition, all the manipulated variables can be incorporated into one control vector and the optimal control vector can be made based on the whole system. An MPC scheme uses a dynamic system model to predict the future behaviour of the system and generates an optimal control vector that minimizes an objective function over the prediction horizon in the presence of disturbances and technical operational constraints. The dynamic energy prices can be incorporated into the MPC controller as well. Therefore, for a DC waste heat-based heat prosumer with TES whose energy bill involves dynamic heating and electricity prices, the MPC can be used to obtain its best possible economic performance while satisfying the required technical operational constraints. However, building an MPC scheme to control a DH system is a complex task, and this is why most previous MPC research was dedicated to the HVAC systems of single buildings [20]. The implementation of MPC at the district level, i.e. the control of the energy supplied to a cluster of buildings has not yet been fully explored [21]. Nevertheless, as pointed out in [22], an MPC scheme is a promising optimal control strategy to meet the requirements of robustness, efficiency and scalability for the controller of a DH network. Despite the inherent difficulties, several researchers still proved the feasibility of the MPC application in DH systems. Verrilli et al. designed an MPC controller to optimize the operation of a DH system that integrates TES and uses a combined heat and power (CHP) plant as a heat source. The designed MPC focused on reducing the operating and maintenance cost of the CHP plant by scheduling boilers, TES units, and flexible loads. The proposed approach was tested using the data obtained from a DH system in Finland by both simulation and experiment methods, and the results showed the cost benefits of the approach [23]. Moreover, Saletti et al. developed an MPC controller to optimize the management and heat distribution of the CHP in a DH system by utilizing the thermal capacity of the connected buildings as TES. The approach was tested on a DH system located in central Sweden, and one week's simulation results demonstrated the effectiveness of the MPC with a peak load shaving of 16% and a mass flow rate reduction of 23% [24]. Furthermore, Hermansen et al. proposed an MPC strategy for a heat booster substation in an ultra-low temperature DH system to minimize the operation costs of the heat pump, which was used to charge the TES, by optimizing the charging schedule of the TES. The proposed MPC strategy was successfully implemented in a real DH system in Copenhagen to verify the control strategy [25]. Lyons et al. proposed an MPC approach with reduced-order models [26]. These reduced-order models were tractable even for centralised MPC formulations with large numbers of buildings. The approach was tested by a case study of 95 dwellings connected to a single heat source. Aoun et al. studied a Mixed

Integer Linear Programming MPC strategy for the buildings connected to DH systems [27]. The MPC strategy exploited the thermal inertia of buildings for short-term TES. Numerical simulation showed that, compared to conventional weather-compensation control, the MPC proved to be cost-efficient, while preserving a decent indoor thermal comfort level. Leitner et al. applied MPC to operate electric heaters for low-temperature DH systems [28]. The method was tested on a system model with model components of a water tank TES, a heat exchanger and pipelines. Simulation results showed that the MPC reduced peak heat and electricity demands compared with the reference controller. However, the limited literature shows that MPC is commonly used to optimize the operation of a DH system with a single heat production plant, like a CHP plant. Research on the DH system with multiple heat sources, especially on the DH system integrated with DC waste heat and TES, is hard to find. The challenge is that the DH systems with multiple heat sources are much more complex than the DH systems with a single heat source, which makes the already complex modelling and control design method of the MPC schemes even more complicated.

To overcome the above limitations and fill the knowledge gap, this study aimed to use an MPC scheme to realize the optimal control of the DC waste heat-based heat prosumer with TES. An MPC scheme that employed an economic-related objective function was proposed, and both the economic boundary and the technical operational constraints were formulated for this MPC scheme. The economic boundary was proposed by considering the heating and electricity pricing mechanism in Nordic countries simultaneously, and the technical operational constraints were defined by using the real measured data of the case system. The proposed MPC scheme was tested by simulation on a campus DH system in Norway, which was a DC waste heat-based heat prosumer. The case system was monitored by the university energy management platform, and extensive operational data were available to aid the study. The proposed MPC scheme together with a conventional rule-based control (RBC) strategy was evaluated in terms of DC performance, local DH system performance, and the overall performance of heat prosumer. The novelty of this study is summarized as the following. Firstly, this research aimed to explore an optimal control strategy for the DC waste heat-based heat prosumer with TES, which is a practical yet rarely addressed problem. Secondly, an MPC scheme was used to maximize the economic performance of a DH system by fully exploring the flexibilities of the system and thereby it may enrich the research on the implementation of MPC at a district level, especially for the DH systems with multiple heat sources. Thirdly, the dynamic pricing schemes of heating and electricity were considered simultaneously to formulate the economic boundary, which

may contribute to the research on the energy system coupling thermal and electrical networks. Finally, real measured operational data was used to define the technical operational constraints, which may supplement the reference values provided in standards and reveal the practical operation of the case system.

This article is developed from our previous studies presented in [6, 29, 30]. As primary research, [6, 29, 30] has been focusing on modelling and system design. This paper adopts the system models and the selected system configuration from [6, 29, 30], while further solving the optimal operation and control problems. The remainder of this article is organised as follows. Section 2 introduces a typical DC waste heat-based heat prosumer with short-term TES, the developed method of economic boundary, the modelling method of the system, and the formulation method for MPC. Section 3 introduces the case study and provides information on simulation settings and research scenarios. Section 4 presents the model validation and the simulation results. Finally, Section 5 concludes this study.

2. Method

This section first introduces a typical DC waste heat-based heat prosumer with short-term TES and then elaborates on the economic boundary condition and the system modelling method. Finally, the formulation of MPC is illustrated.

2.1. Typical data centre waste heat-based heat prosumer with short-term thermal energy storage

Fig. 1 illustrates a typical DC waste heat-based heat prosumer with short-term TES. A water tank thermal energy storage (WTTES) was chosen as the short-term TES in this study, because it is easily implemented and economically reasonable for DH systems [6, 31]. A main substation (MS) is usually used to connect the city DH network with the distribution network of heat prosumer and to physically separate the flows so that the local DH system of heat prosumer can be managed independently from its city DH network. There are two heat exchangers (HEs) in the MS, HE1 is used to charge the WTTES and HE2 is used to supply heat from the city DH network to the heat prosumer's local DH network. An HP was used to cool down the DC by utilizing the HP evaporator and to harvest the DC waste heat for the heat prosumer's local DH network by utilizing the HP condenser, as shown in Fig. 1. There are usually two common connection ways between the DC and

the DH systems: the return to supply (R2S) and the return to return (R2R) connection. The R2S connection implies that water is extracted from the return pipe, heated to a proper temperature, and then fed into the supply pipe of the DH system. The R2R connection implies that water is extracted from the return pipe and heated to any temperature, because it already has a higher temperature than the return water of the DH system, and fed into the return pipe [9, 32]. In this study, the R2R connection was chosen, because it is preferable for low-temperature heat sources and no extra heat sources are required to raise the temperature of water delivered into the DH system [4, 9]. Finally, a cluster of buildings is the heat user, and a circulator pump (CP) is used to circulate the hot water for the heat prosumer's local DH network.

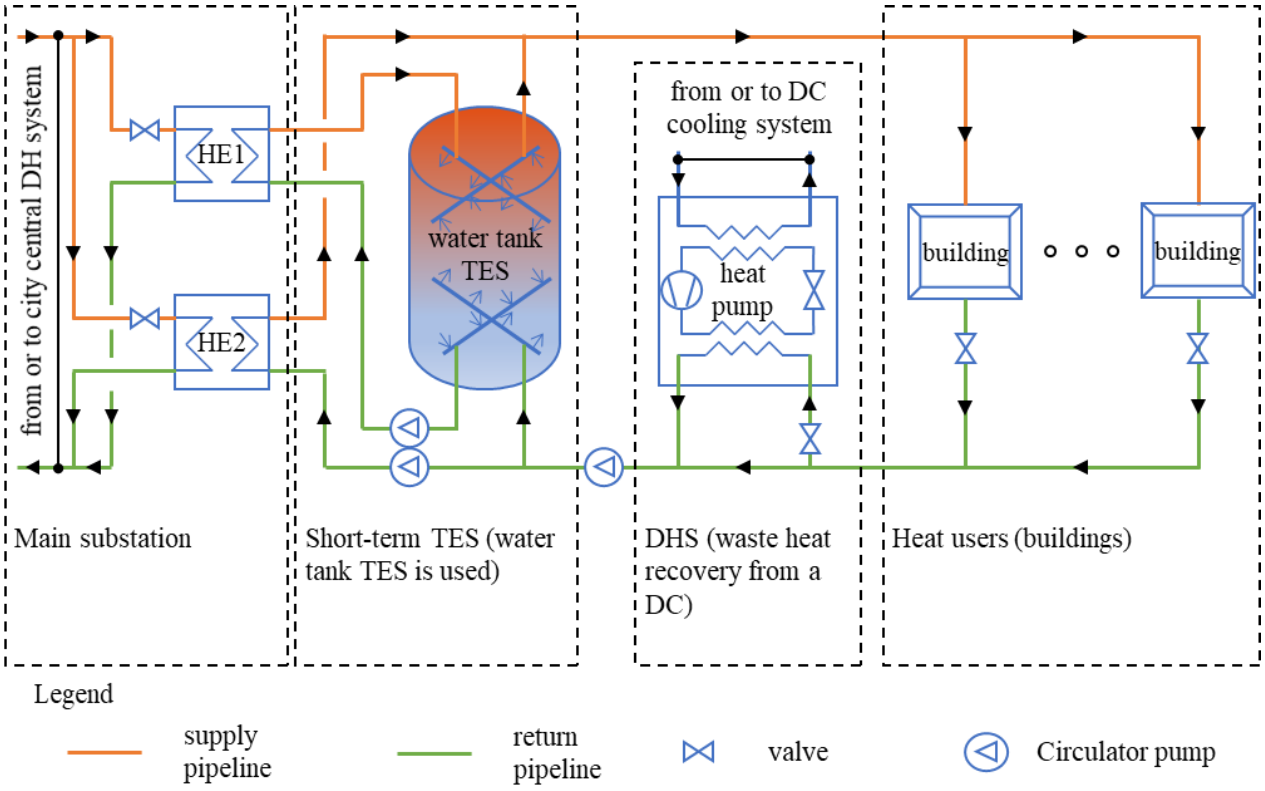

Fig. 1. Typical data centre waste heat-based heat prosumer with short-term thermal energy storage

2.2. Economic boundary

As presented in Fig. 1, the system energy bill comes from two parts: 1) heating bill paid for the DH use and 2) electricity bill paid for the electricity use. The DH company provides heat for the HE1 and HE2 in the MS, and the electricity company provides electricity to power the HP of DC and the CP. Therefore, this section illustrates the economic boundary by considering the pricing

mechanism in Nordic countries for the heating price model and electricity price model simultaneously.

2.2.1 Heating price model

A generalized heating price model has been discussed in detail and proposed in [30]. This generalized heating price model only considered the energy demand component (EDC) and the load demand component (LDC), because the EDC and the LDC are the most commonly used components in the existing heating price models. The EDC is used to cover the DH companies' fuel costs, and it is charged based on the total heat use of heat users. The LDC is typically used to compensate DH companies' costs of maintaining a particular level of capacity for peak load, as well as new facility investment costs, depreciation, and other expenses, and it is charged based on the peak load of the heat users [33]. This study used the same generalized heating price model proposed in [30], which only considered the EDC and the LDC as shown in Equations (1), (2), and (3).

$$C_{hea} = C_{edc} + C_{ldc} \tag{1}$$

$$C_{edc} = \int_{t_0}^{t_f} EP(t) \cdot \dot{Q}(t) \cdot dt \tag{2}$$

$$C_{ldc} = LP \cdot \dot{Q}_p \tag{3}$$

where C_{hea} is the total heating cost. C_{edc} is the EDC and calculated by Equation (2). C_{ldc} is the LDC and calculated by Equation (3). $EP(t)$ and $\dot{Q}(t)$ are the EDC heating price and the heat rate supplied to the heat user at time t, respectively. LP and $\dot{Q}_p$ are the LDC heating price and the peak heat rate. In this study, the units of $EP(t)$ and LP were NOK[1]/kWh and NOK/kW, respectively.

2.2.2 Electricity price model

Although electricity contracts vary from country to country, a generalized electricity price model was proposed in this study. This generalized electricity price model was based on the investigation of electricity contracts in Norway. In Norway, the end-users have to pay for two parts when using electricity: 1) power price for the electricity bought from a power supplier and 2) grid rent to the local grid distribution company for transporting the power. Thereof, the end-users are free to choose any power supplier within the country. The grid company, however, cannot be chosen by

1 The currency rate between NOK and EUR can be found from https://www.xe.com/, in this study 1 EUR=10.0 NOK.

the end-users. There is only one gird distribution company responsible for a certain geographical area [34, 35].

Regarding the power price paid for a power supplier, it is determined by the different contracts provided by the power supplier. It is impossible to distinguish between different power suppliers. What differentiates power suppliers from each other is the contracts they offer. In general, end users can choose between three main types of contracts: fixed-price, variable price and spot price. According to Statistics Norway, the spot-price contract is the most common and widely used contract type in Norway [36]. Therefore, the spot-price contract was used in this study regarding the power price paid for a power supplier. In a spot-price contract, the price follows the market price determined by Nord Pool [37]. A mark-up must also be paid by the customer [38]. The price for the spot-price contract is calculated by Equations (4), (5), and (6).

$$C_{ele\_pow}=C_{spo}+C_{sur}+C_{mfi} \tag{4}$$

$$C_{spo}=\int_{t_0}^{t_f} PP_{spo}(t)\cdot\dot{E}(t)\cdot dt \tag{5}$$

$$C_{sur}=\int_{t_0}^{t_f} PP_{sur}\cdot\dot{E}(t)\cdot dt \tag{6}$$

where C_{ele_pow} is the power price paid for a power supplier. C_{spo} is the spot price-related fee and calculated by Equation (5). C_{sur} is the surcharge-related fee and calculated by Equation (*6*). C_{mfi} is the monthly fixed fee. $PP_{spo}(t)$ is the spot price at time t and obtained from Nord Pool [37]. PP_{sur} is the surcharge including electricity certificate, and $\dot{E}(t)$ is the electricity use at time t. In this study, both the units of $PP_{spo}(t)$ and PP_{sur} were NOK/kWh.

Regarding the grid rent paid for the grid distribution company, it is decided by the local grid distribution company and is strictly regulated by the Norwegian Water Resources and Energy Directorate (NVE). For a big business end-user, the grid rent consists of an energy link fee, a power link fee and an annual fixed link fee [39]. The grid rent price is calculated by Equations (7), (8), and (9).

$$C_{ele\_gri}=C_{ene}+C_{pow}+C_{afi} \tag{7}$$

$$C_{ene}=C_{pow}\int_{t_0}^{t_f} GP_{ene}\cdot\dot{E}(t)\cdot dt \tag{8}$$

$$C_{pow}=GP_{pow}\cdot\dot{E}_p \quad (9)$$

where C_{ele_gri} is the grid rent paid for the local grid distribution company. C_{ene} is the energy link fee and calculated by Equation (8). C_{pow} is the power link fee and calculated by Equation (9). C_{afi} is the annual fixed fee. GP_{ene} is the energy link fee per energy unit, and $\dot{E}(t)$ is the electricity use at time t. GP_{pow} is the power extraction price per power unit, and $\dot{E}_p$ is the highest hourly power output. In this study, the units of GP_{ene} and GP_{pow} were NOK/kWh and NOK/kW, respectively.

Finally, a generalized electricity price model was proposed in this study based on the above explanation, and it is calculated as Equation (10).

$$C_{ele}=C_{ele\_pow}+C_{ele\_gri} \quad (10)$$

where C_{ele} is the total electricity cost, C_{ele_pow} is the power price paid for a power supplier as shown in Equation (4), and C_{ele_gri} is the grid rent paid for the local grid distribution company as shown in Equation (7).

2.3. System modelling

MPC inherently requires an appropriate dynamic system model, which is used to predict the future behaviour of the system and calculate the optimal manipulated variable trajectory. In this study, the system dynamic model was developed using the Modelica language, and it was based on the energy and mass flow exchanging connection between the individual component model. As shown in Fig. 1, a typical DC waste heat-based heat prosumer with WTTES includes the individual component of the WTTES, DC, buildings, CP, and pipelines. The energy and mass flow exchanging between these components and the modelling method for the individual component of the WTTES, buildings and pipelines are briefly presented in Sections Appendix A- Appendix D, yet the more detailed information is elaborated in the research [30]. This section focuses on the modelling method for the individual component of the DC and the CP.

2.3.1 Model for data centre

An HP was used to cool down the DC by utilizing the HP evaporator and to harvest the DC waste heat for the DH system by utilizing the HP condenser. Fig. 2 illustrates the basic components of the HP. There are mainly two types of HP models in existing studies: 1) theoretical model and 2) empirical model [40-43]. Thereof, the empirical model is usually developed based on measured data

rather than simulating the details of HP, and it is widely used for energy performance assessment of an HP [41, 43]. Therefore, an empirical HP model was developed in this study, because there were extensive available measured data for the case system and the developed HP model was mainly used for the energy use prediction.

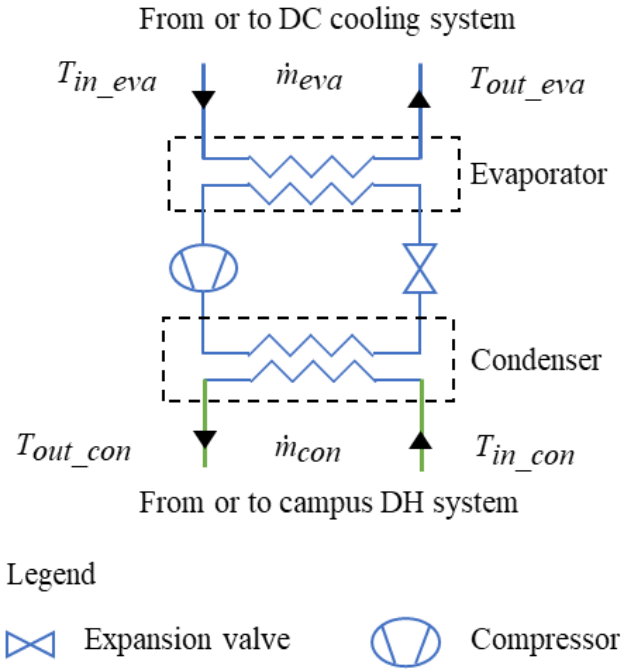

Fig. 2. The heat pump used to capture waste heat from the data centre

Except for the inherent performance characteristics of the HP, the operational conditions are the main factors that influence the energy performance of an HP [44]. The operational conditions include the inlet and outlet water temperature and the water mass flow rate on the evaporator and condenser sides of an HP [45]. Therefore, the HP compressor power may be expressed by a simple function involving the above mentioned operational conditions, as shown in Equation (11):

$$\widehat{E}_{HP}=a\cdot T_{in\_eva}+b\cdot T_{out\_eva}+c\cdot T_{in\_con}+d\cdot T_{out\_con}+e\cdot \dot{m}_{eva}+f\cdot \dot{m}_{con} \quad (11)$$

where $\widehat{E}_{HP}$ is the simulated compressor power. T_{in} and T_{out} are the inlet and outlet water temperatures. $\dot{m}$ is the water mass flow rate. Subscripts *eva* and *con* are the evaporator and the condenser. All the above-introduced variables have been marked in Fig. 2. Moreover, a, b, c, d, e, and f are the parameters needed to be identified. In this study, the HP compressor power as well as operational conditions, including the inlet and outlet water temperature and the water mass flow rate on the evaporator and condenser sides of the HP, were measured every 10 minutes. These measured data

were used to identify the parameters (a, b, c, d, e, and f) by solving the following optimization problem.

Minimize:

$$\sum_{k=1} (\widehat{E}_{HP,k}-E_{HP,k})^2 \tag{12}$$

subject to:

$$z_L \leq z_k \leq z_U \tag{13}$$

where $\widehat{E}_{HP,k}$ is the simulated compressor power as described by Equation (11). $E_{HP,k}$ is the measured compressor power. The vector z_k is the set of the parameters needed to be identified. z_L and z_U are the lower and the upper limits for these parameters. Finally, the Evolutionary engine provided by the Excel Solver was used in this study to solve the optimization problem and obtain the parameter values.

2.3.2 Model for circulator pump

A CP was used to circulate the warm water for the heat prosumer's local DH network and overcome pipeline hydraulic resistance and local pipeline accessory resistance. A variable-speed circulator pump was used in this study because it has the potential to significantly reduce pumping energy use [46]. The total pumping power required to circulate the water in a distribution system can be calculated by using Equation (14) [2] as:

$$P_{CP}=\frac{\Delta P \cdot \dot{V}}{\eta_{CP}} \tag{14}$$

where $\dot{V}$ is the volume flow rate of water, and η_{CP} is the total conversion efficiency for the CP that was obtained from CP manufacturers and was 0.7 at the design condition in this study [47]. ΔP is the total pressure drop of the DH pipeline network and can be calculated by Equation (15) [2] as:

$$\Delta P=S \cdot \dot{m}^2 \tag{15}$$

where $\dot{m}$ is the water mass flow rate. S is the resistance friction coefficient of the DH pipeline network, which is related to the characteristics of the pipeline. Due to the lack of distribution network characteristics and measured data, one assumption was made in this study: the water flow rate was controlled by the variable-speed CP and the valves of the pipelines had no actions. Therefore, the

resistance friction coefficient S was a constant value and can be deduced from the design condition of the DH system. Meanwhile, the law of similarity of CP was used to obtain the pumping power.

2.4. Formulation of model predictive control

In this study, the MPC scheme employed an economic-related objective function to maximize the heat prosumer's economic performance. The heating and electricity price models described in Section 2.2 were involved in this objective function as shown in Equation (16). However, the monthly fixed fee involved in the power price and the annual fixed fee involved in grid rent were not included, because they are not related to real-time electricity use. In addition, the power link fee involved in the grid rent of electricity price model was not considered as well. This is because only the electricity use for the HP and CP was involved in the optimization problem, the electricity use for other equipment, lighting, etc. was not involved, but the power link fee is charged based on the highest hourly total electricity use of the whole energy system. Therefore, at each time step, the MPC controller solves the following optimization problem:

Minimize:

$$\int_0^H EP(t)\cdot\dot{Q}_{MS}(t)\cdot dt + LP\cdot\dot{Q}_{MS\_p} + \int_0^H (PP_{spo}(t)+PP_{sur}+GP_{ene})\cdot(\dot{E}_{HP}(t)+\dot{E}_{CP}(t))\cdot dt \quad (16)$$

subject to:

$$\dot{Q}_{MS}(t)\leq\dot{Q}_{MS\_p} \quad (17)$$

$$F(t,\boldsymbol{z}(t))=0 \quad (18)$$

$$F_0(t_0,\boldsymbol{z}(t_0))=0 \quad (19)$$

$$z_L\leq\boldsymbol{z}(t)\leq z_U \quad (20)$$

where H is the predictive horizon, which was 12 hours in this study. $\dot{Q}_{MS}(t)$ is the heat flow rate of MS at time t. $\dot{Q}_{MS\_p}$ is the peak heat rate of MS, and it was a parameter to be optimized in this study. The peak heat rate was defined as the maximum hourly heat use during one month in this study according to the research [48]. $EP(t)$, LP, $PP_{spo}(t)$, PP_{sur} and GP_{ene} have been explained in Section 2.2. Moreover, $\dot{E}_{HP}(t)$ and $\dot{E}_{CP}(t)$ are the electricity use of the HP and CP at time t, respectively. The equality constraints of Equation (18) and Equation (19) are the system dynamics as explained in Section 2.3 and the initial condition of the system, respectively. Finally, Equation (20) defines the inequality constraint including the technical operational constraints. $\boldsymbol{z}\in R^{n_z}$ is the set of time-

dependent variables, which includes the manipulated variables $\boldsymbol{u} \in R^{n_u}$ to be optimized, the differential variables $\boldsymbol{x} \in R^{n_x}$, and the algebraic variables $\boldsymbol{y} \in R^{n_y}$. $z_L \in [-\infty, \infty]^{n_z}$ and $z_U \in [-\infty, \infty]^{n_z}$ are the lower and upper limits, respectively.

The above-formulated optimization problem was solved on the optimization platform JModelica.org [49]. The optimization algorithm used in JModelica.org is explained as follows. The formulated infinite-dimensional optimization problem was discretized into a finite-dimensional nonlinear programming (NLP) problem by using a direct collocation method [50, 51]. Afterwards, the discretized finite-dimensional NLP problem was solved using the NLP solver, Interior Point Optimizer (IPOPT), by the following steps. Firstly, the interior-point method was used to eliminate the inequality constraints of the NLP problem. Then, using Newton's iteration method, a local optimized manipulated variable trajectory was obtained by solving Karush-Kuhn-Tucker conditions.

3. Case study

The method proposed in Section 2 was tested by simulation on a campus DH system in Norway. The background of the case study, simulation settings and research scenarios are explained in this section.

3.1. Background of the case study

The case study was a campus DH system in Trondheim, Norway, as presented in Fig. 3. There is an MS to connect the campus DH system with the city DH network via HEs, and hence the campus DH system can be managed independently. A DC acts as a DHS because the return water of the campus DH network is used to harvest the DC's waste heat by cooling down the high-temperature refrigerant vapour at the HP condenser. The heat users in this campus DH system are buildings whose total building area is about 300 000 m², and more detailed information about the buildings can be found in research [52]. According to the measurement data from June 2017 to May 2018, as shown in Fig. 4, the total heating demand of the buildings was 32.8 GWh. The DC provided around 20% heat for buildings, while the rest 80% of the heat was supplied from the city DH network via the MS. Therefore, this campus DH system is a DC waste heat-based heat prosumer.

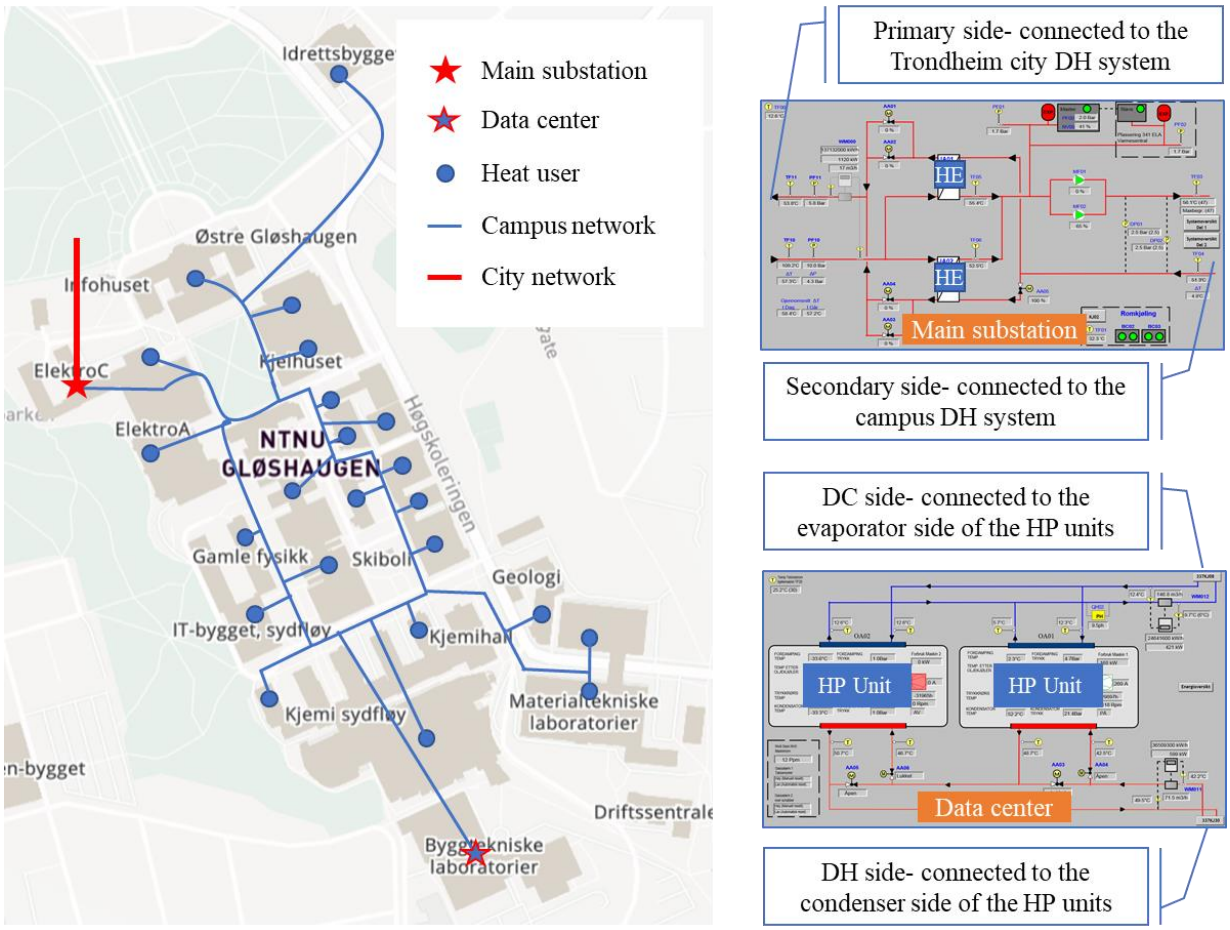

Fig. 3. Campus district heating system

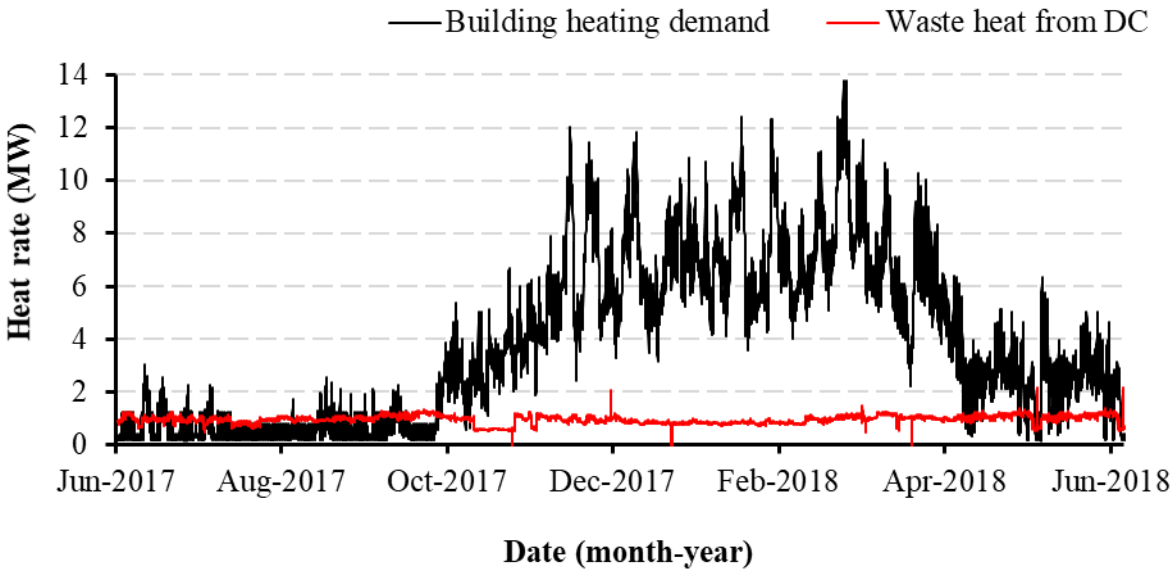

Fig. 4. Heating demand and waste heat recovery of the campus district heating system

Another phenomenon observed from Fig. 4 is that the buildings' heating demand was not evenly distributed and there were high peak loads from the MS, especially for the heating season. The heating price model adopted by the local DH company takes peak loads into account, and the peak load-related heating cost, LDC, accounted for about 26% of the total heating cost each year. Previous research has proven that introducing a short-term TES, WTTES, for the case system was able to address the high peak load problem and improve the system's economic performance [6]. Moreover, an in-depth investigation for the optimal storage size of WTTES has been conducted in research [30]. Therefore, considering the trade-off between investment and heating cost saving, a WTTES with a storage volume of 900 m^3, which was able to supply heat to the campus DH system for up to 12 hours, was introduced in this study.

3.2. Simulation settings and research scenarios

This research was a simulation-based study under the heating season (from October to April) of the year 2017- 2018. The heating season was divided into two periods to investigate, the transitional period and the midwinter period, due to the following reasons. Firstly, the heating demand in October and April were much smaller than that from November to March. The average heating demand in October and April were 2.6 and 3.4 MW, respectively, while the average heating demands from November to March were in the range of 5.7- 7.7 MW. Secondly, the average hourly heating demand profile was different in October and April from that from November to March, as shown in Fig. 5. The average heating demand in Fig. 5 was obtained by averaging all the heating demand at the same hour during the midwinter period and the transitional period, respectively.

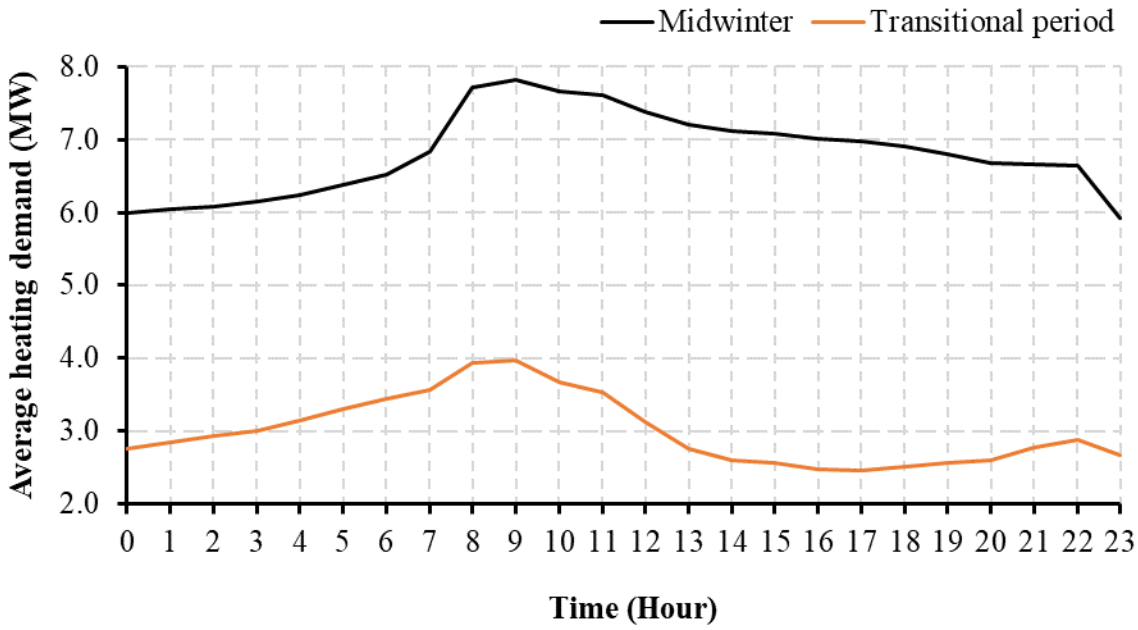

Fig. 5. Average heating demand for each hour during the midwinter and transitional period

Other simulation settings are explained as follows. The building's heating demand came from the measured data as shown in Fig. 4 and was directly used as input in this study. The energy price including heating price and electricity price was obtained from the local DH company's website [53] and a power supplier's website [54]. The used LDC of the heating price was 39 NOK/kW. The used EDC of the heating price varied between 0.484- 0.868 NOK/kWh, and the electricity use-related electricity price fluctuated from 0.485 to 0.870 NOK/kWh.

Two research scenarios were proposed to evaluate the MPC scheme. The operation principles for the two scenarios are presented in Table 1. The reference scenario was based on an RBC strategy, as shown in Fig. 6. A weather compensation controller (WCC) was used to control the supply water temperature of HE2 based on the outdoor air temperature. The water flow rate of HE2 was adjusted by a proportional-integral (PI) controller based on the feedback of return water temperature. The reference values of the return water temperature were obtained by the linear regression based on measured data, as explained in [30]. Another PI controller was used to determine the HP compressor power based on the feedback of the outlet water temperature of the evaporator. The reference value of the outlet water temperature of the evaporator was set as 6.5℃ because most of the measured outlet temperature of the evaporator fluctuated between 6 and 7℃ and the average value was 6.5℃. Finally, the charging and discharging processes of the WTTES were decided by a pre-defined schedule

presented in Table 2. The schedule was made based on the average hourly heating demand profile during the transitional and the midwinter period, respectively, as shown in Fig. 5. In the schedule, the charging heat rate was realized by maintaining the supply temperature of HE1 at 80℃ and adjusting the water flow rate of HE1, while the discharging heat rate was achieved by adjusting the water flow rate of the WTTES.

Table 1. The operation principles for the two scenarios

		Rule-based control scenario	**Model predictive control scenario**
Input variables	Outdoor air temperature	Yes	No
	Heat demand	No	Yes
	Energy price	No	Yes
Manipulated variables	Supply temperature of HE1	Maintain at 80℃	Decided by the MPC controller
	Water mass flow rate of HE1	Adjusted based on charging heat rate	Decided by the MPC controller
	Supply temperature of HE2	Decided by the WCC controller	Decided by the MPC controller
	Water mass flow rate of HE2	Decided by the PI controller 1	Decided by the MPC controller
	Water mass flow rate of WTTES	Adjusted based on discharging heat rate	Decided by the MPC controller
	Power of HP compressor	Decided by the PI controller 2	Decided by the MPC controller

Table 2. The schedule of charging and discharging process of water tank thermal energy storage in the rule-based control scenario

Month	**Discharging process**	**Charging process**	**Charging/ Discharging heat rate** (MW)
October, April	5:00 - 12:00	21:00 - 4:00	0.5
November- March	7:00 - 17:00	22:00 – 6:00	1.0

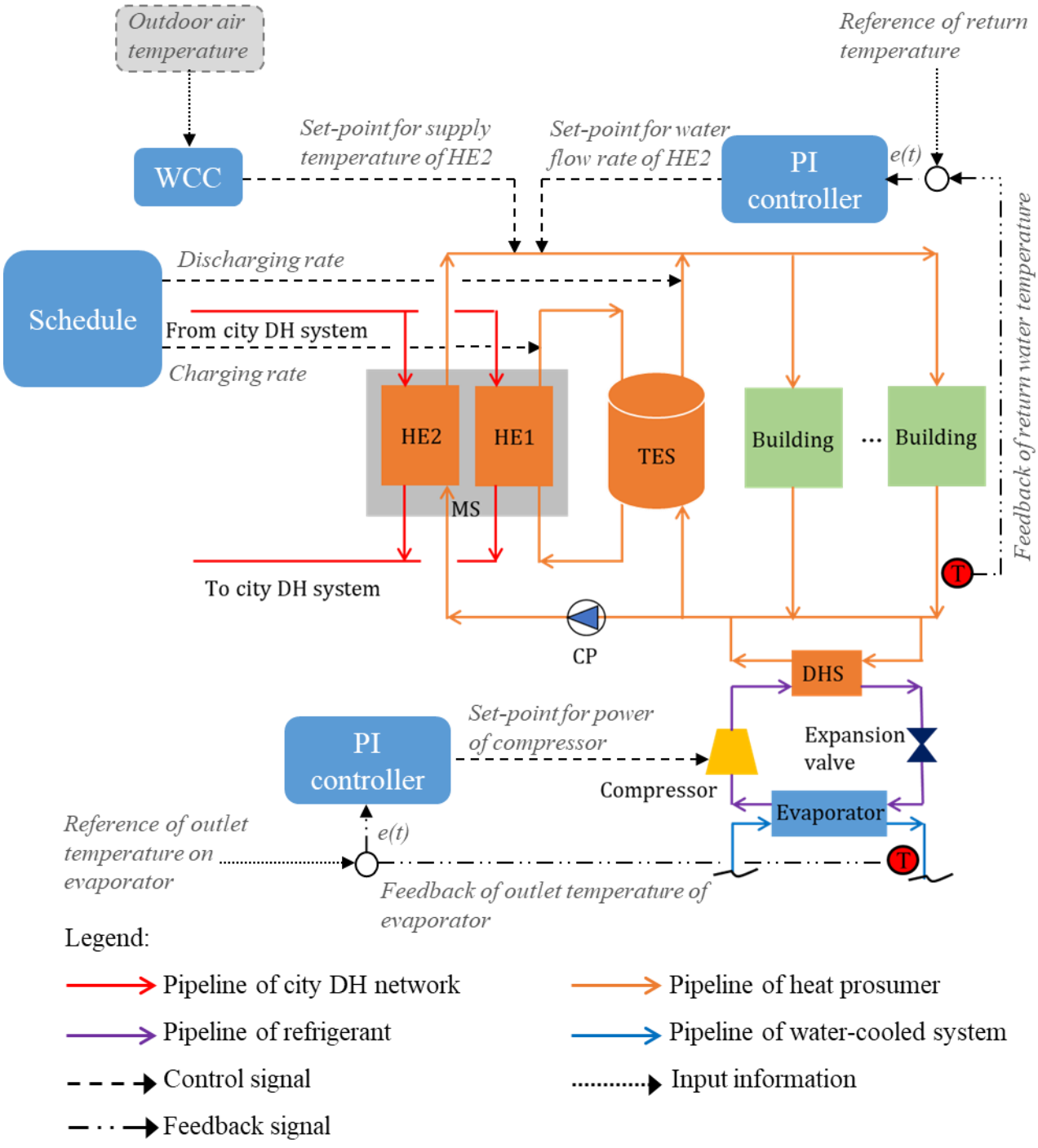

Fig. 6. The scenario of rule-based control

The MPC scenario was based on the MPC scheme proposed in Section 2.4 both during the transitional and midwinter period, as illustrated in Fig. 7. In this scenario, the building's heating demand and the energy price over the predictive horizon were incorporated into the MPC controller. The controller evaluated the objective function with various manipulated variable trajectories until

an optimal trajectory was found. As presented in Fig. 7, the manipulated variables were the supply water temperature and mass flow rate of the HEs, the water mass flow rate of the WTTES and the power of the HP compressor. These manipulated variables were constrained to their feasible regions in the real system, which formulates the technique operational constraints of the MPC. The constraint settings for the supply water temperature and water mass flow rate of the HEs, and the water mass flow rate of the WTTES were elaborated in the research [30]. Moreover, the upper bound and lower bound of the HP compressor power were defined by the measured data. Another critical operational constraint was that the DC cooling requirement had to be satisfied. In this study, the DC cooling requirement was guaranteed by maintaining the outlet water temperature of the evaporator in the range of 6 - 7℃, because the measured inlet water temperature and mass flow of the evaporator were almost constant values while most of the measured outlet water temperature of the evaporator fluctuated in the range of 6- 7℃.

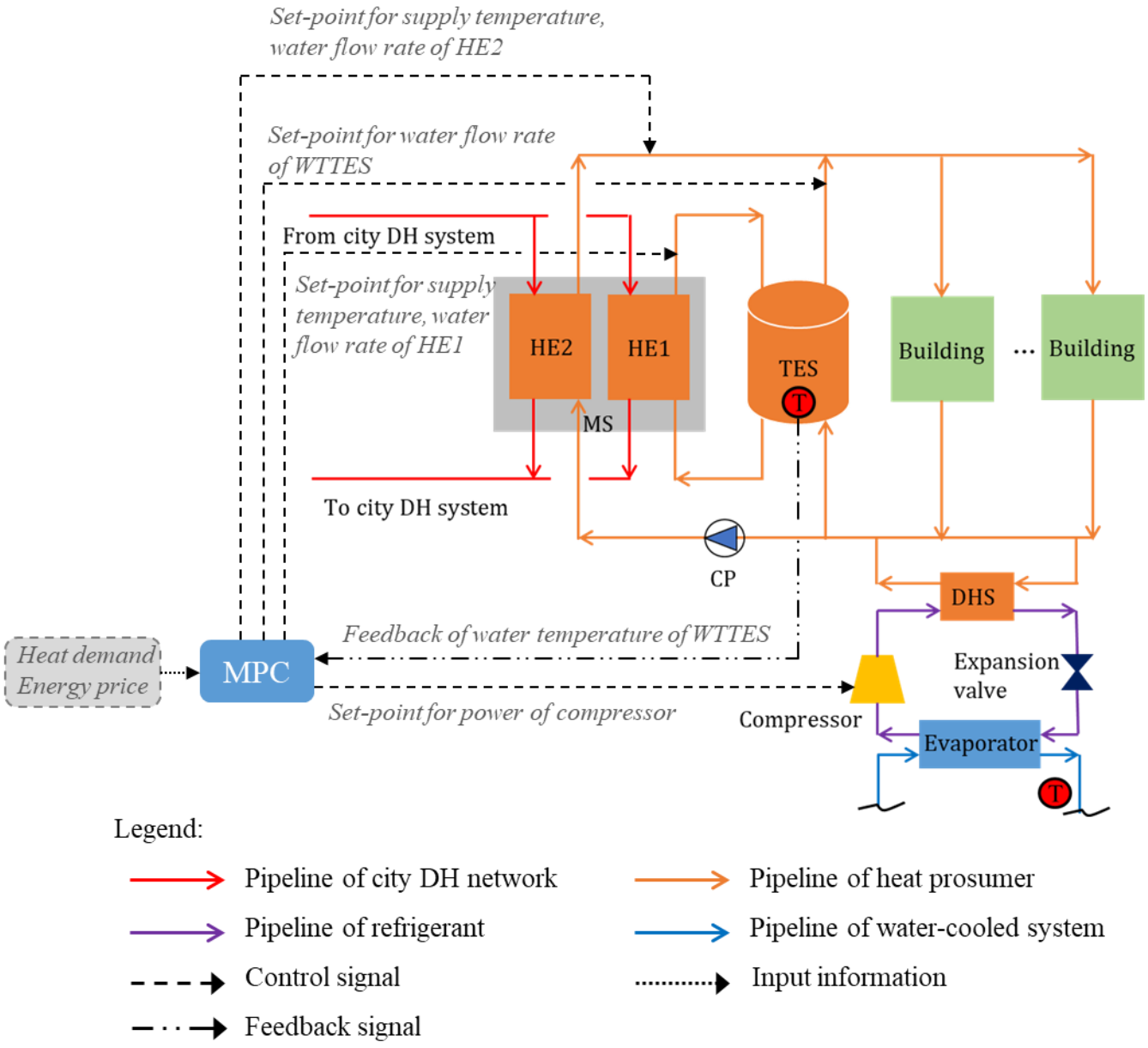

Fig. 7. The scenario of model predictive control

4. Results

This section first presents the model validation, and then evaluate the MPC scheme in terms of the DC performance, the local DH system performance, and the overall performance of the heat prosumer. In addition, January and April of 2018 were chosen as the typical month for the midwinter and the transitional period, respectively, to conduct the simulation-based study.

4.1. Model validation

This section mainly presents the model validation of the DC, because the model validation of the other individual component, such as the WTTES and the pipelines, has been elaborated in the previous research [30].

The identified parameter values for the DC model are presented in Table 3. This developed DC model was validated against the measured data from the university energy management platform, as shown in Fig. 8. To quantify the deviation between the simulated and the measured compressor power, three indicators, i.e., mean absolute error (MAE), mean absolute percentage error (MAPE) and root mean square error (RMSE) were used to evaluate the prediction performance of the model [55, 56]. The resulted values of these indicators are shown in Fig. 8. In addition, Fig. 8 presents that the simulated compressor hourly power matched with the measured data well, with the coefficient of determination (R^2) of 0.93 and no obvious overfitting.

Table 3. Identified parameters for data centre model

Parameter	*a*	*b*	*c*	*d*	*e*	*f*
Value	-1.54	10.55	-16.98	24.40	-5.74	-9.32

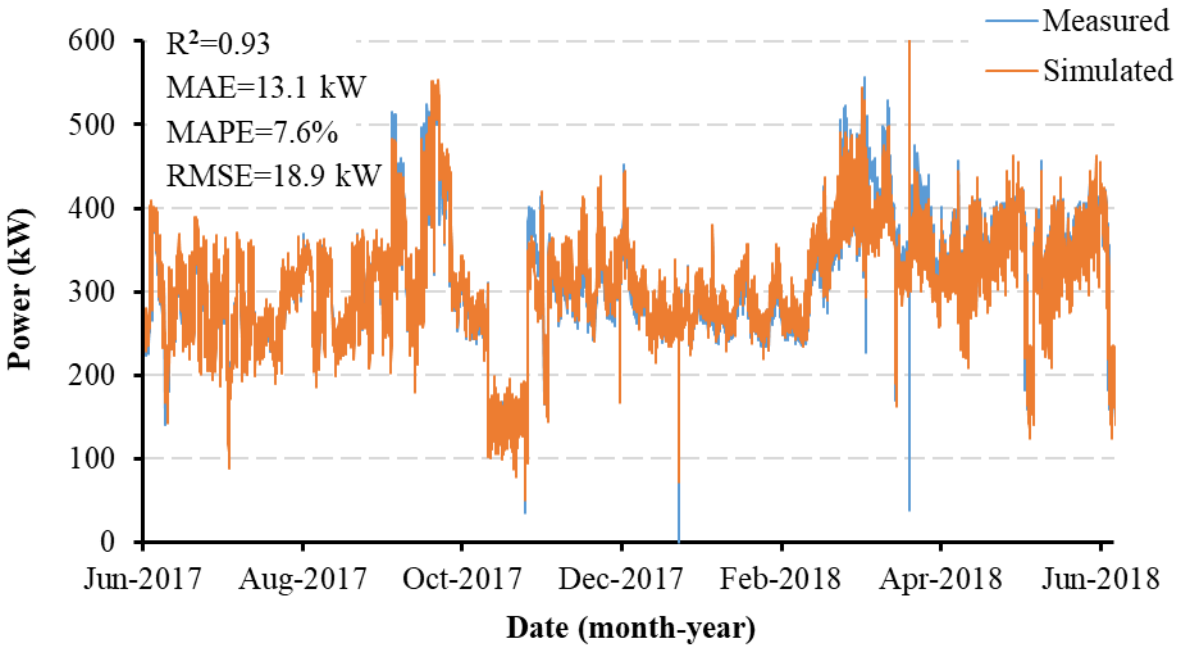

Fig. 8. Simulated and measured hourly power of the compressor of heat pump

4.2. Data centre performance

The outlet temperature of the evaporator, the coefficient of performance (COP) of the HP, and the electricity use of the HP were used as indicators to evaluate the DC performance. Firstly, Fig. 9 presents the outlet temperature of the evaporator in January and April, respectively. Two obvious phenomena can be observed from Fig. 9: 1) Both the MPC scenarios had smaller outlet temperature fluctuating ranges compared to the RBC scenarios, especially in April; 2) Both the MPC scenarios preferred lower outlet temperatures with average values of 6.0 and 6.1℃, respectively. The average values of the outlet temperatures were 6.5℃ in the RBC scenarios. Moreover, one conclusion was obtained as well: the cooling requirement of DC was satisfied in both MPC and RBC scenarios, because most of the outlet water temperatures of the evaporator were within its feasible region from 6.0 to 7.0℃.

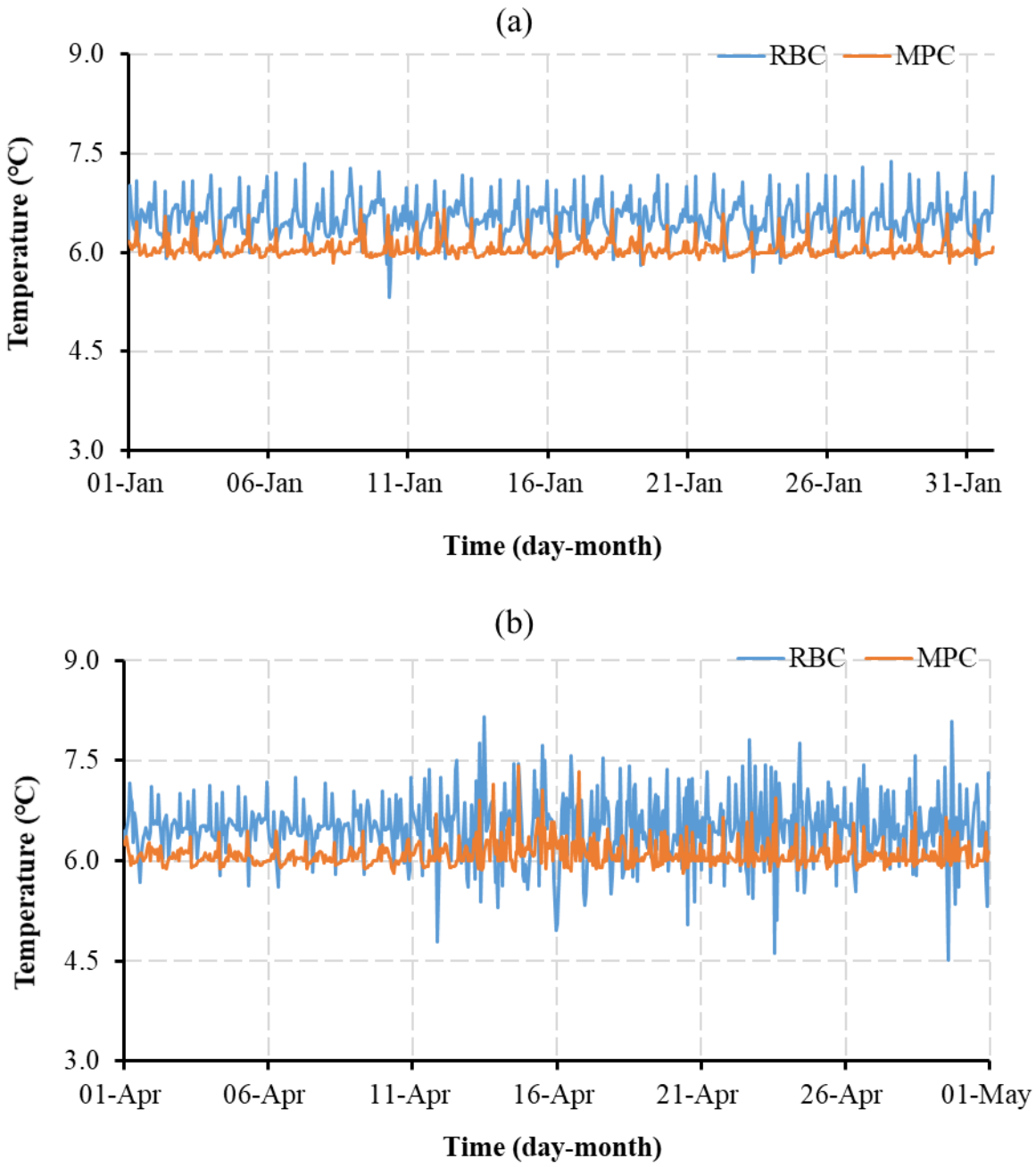

Fig. 9. Simulated outlet temperature of evaporators (a) January of 2018 (b) April of 2018

Fig. 10 presents the COPs of HP in January and April. Similar to the outlet temperature of the evaporator, the COPs of the HP in the MPC scenarios varied within a smaller range compared to the RBC scenarios, especially in April. The COPs of the HP in the MPC scenario varied within the range of 2.3 to 3.3 in April, while that of the range in the RBC scenario was 2.4 to 3.8, as presented in Fig. 10 (b). In terms of the average value of COP, the MPC scenario was higher than that of the RBC

scenario in January, with values of 3.1 and 2.9 respectively. However, the average value of COP in the RBC scenario was a bit higher than that of the MPC scenario in April, with values of 3.1 and 3.0 respectively. These results indicated that the MPC scheme was more robust than the RBC scheme expressed as the smaller fluctuating ranges of both the outlet temperature of the evaporator and the COP of the HP, which are crucial for the DC cooling system's safe operation.

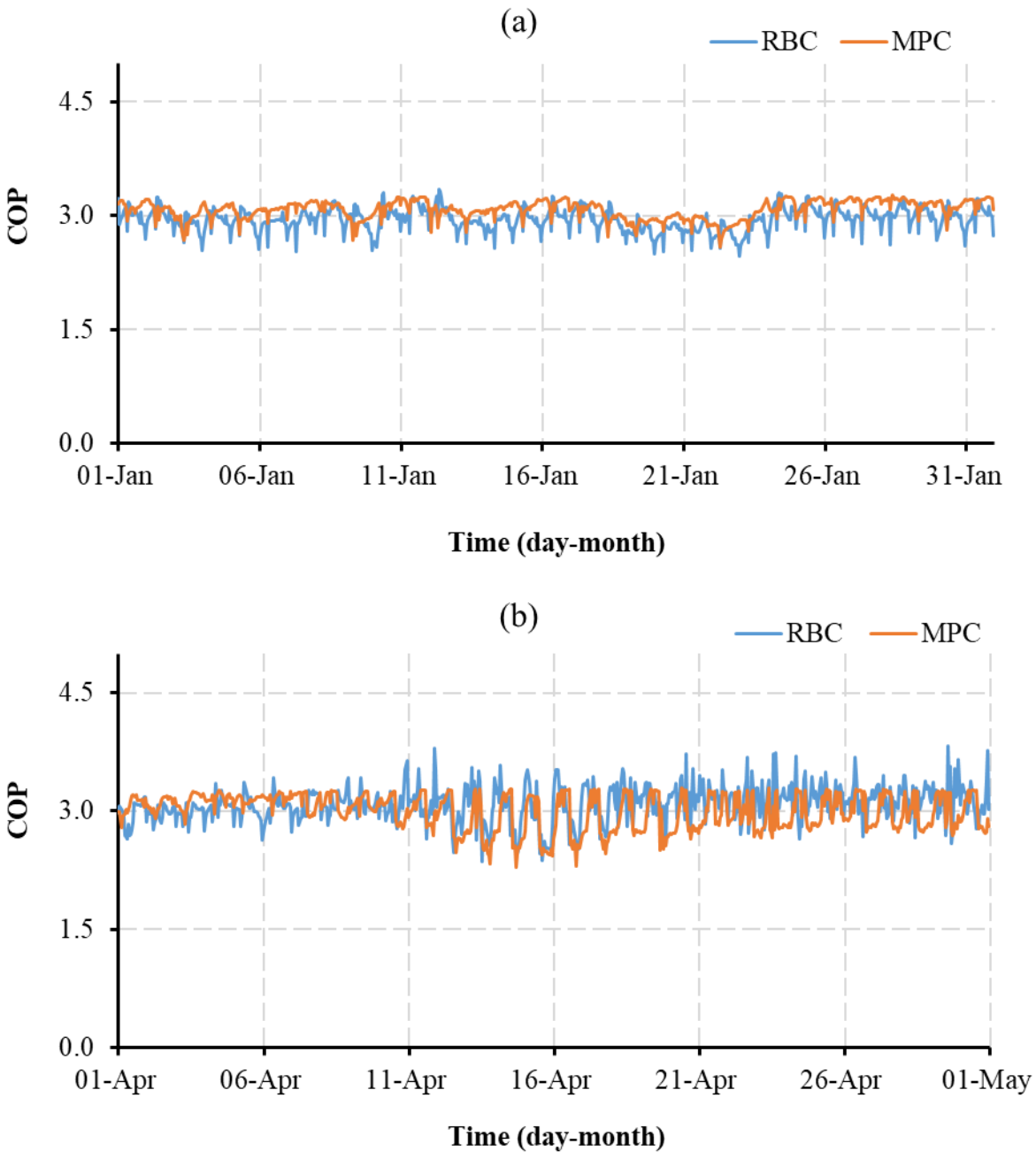

Fig. 10. Simulated coefficient of performance of heat pumps (a) January of 2018 (b) April of 2018

One phenomenon that can be noticed from the above results is that both the changing range of the evaporator outlet temperature and COPs of HP in April was higher than that in January. This can be explained by the following. For an optimization problem, the optimization results are strongly dependent on the inputs of the optimization problem. In this study, the heating demand was a key input for the optimization problem, and the heating demands in January and April are shown in Fig. 4. Firstly, the heating demand in April had a larger changing range than that in January. Secondly, the heating demand in April could be lower or higher than the DC waste heat supply (1 MW), while the heating demand in January was more stable and higher than the DC waste heat supply. Finally, this resulted in the control situation in April being more complicated. These two characteristics of heating demand in January and April resulted in their corresponding different results.

Fig. 11 presents the monthly electricity use of the HP for two scenarios, respectively. Two main phenomena can be noticed from Fig. 11: 1) The MPC scenarios used more electricity for HPs than the RBC scenarios in both January and April; 2) The electricity use of the HP in the MPC scenarios had no big difference in January and April, while the RBC scenario used much more electricity in January than in April. These phenomena indicated that the electricity use of the HP in the MPC scenarios was much more stable, and the MPC scenarios preferred to generate more waste heat from the HP by using more electricity because the COPs of the HP were always higher than 1.0 and maintained at around 3.0-3.1. More explanation will be shown in Section 4.4. Moreover, this may be the reason why the MPC scenarios preferred the lower outlet temperatures of the evaporator as well.

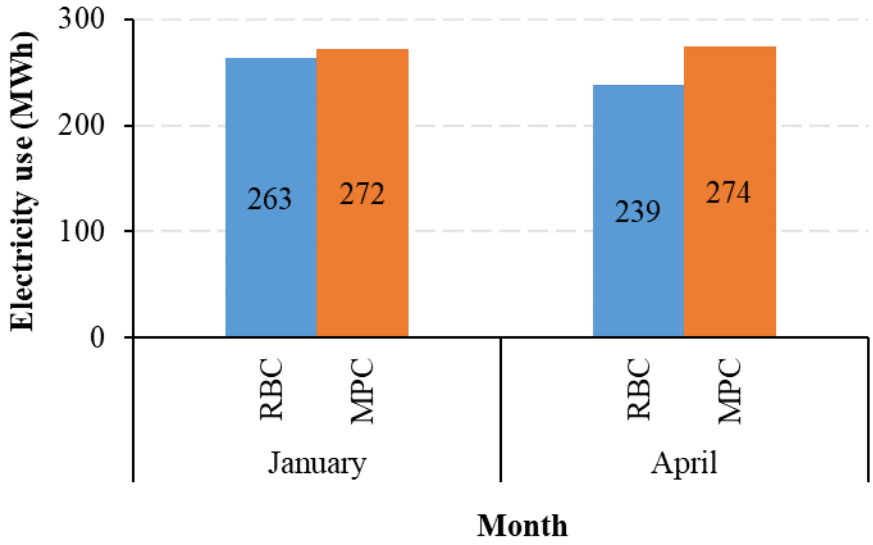

Fig. 11. Simulated electricity use of heat pump

4.3. Local district heating system performance

Peak heat rate and heat use were chosen as the indicators to evaluate the performance of the local DH system. Fig. 12 presents the peak load of the MS for the two scenarios in January and April, respectively. As shown in Fig. 12, both MPC scenarios, in January and April, took better advantage of the WTTES flexibilities, which was demonstrated by the lower peak loads compared to their corresponding RBC scenarios. In January, the peak load of the MPC scenario dropped to around 10.9 MW, a reduction of about 5.6% compared to the RBC scenario. In April, the peak load reduction of the MPC scenario was even more, with a reduction of almost 12.0% compared to the RBC scenario. Fig. 13 presents the heat use of the local DH system for two scenarios in January and April, respectively. As shown in Fig. 13, each MPC scenario saved the heat use compared to its corresponding RBC scenario, with savings of 2.0% and 3.7%, respectively.

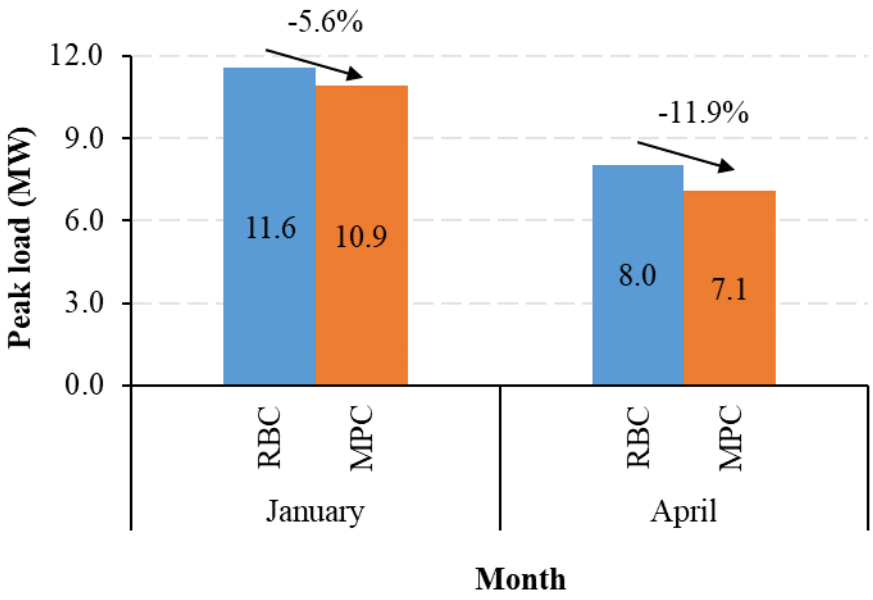

Fig. 12. Simulated peak load for two scenarios

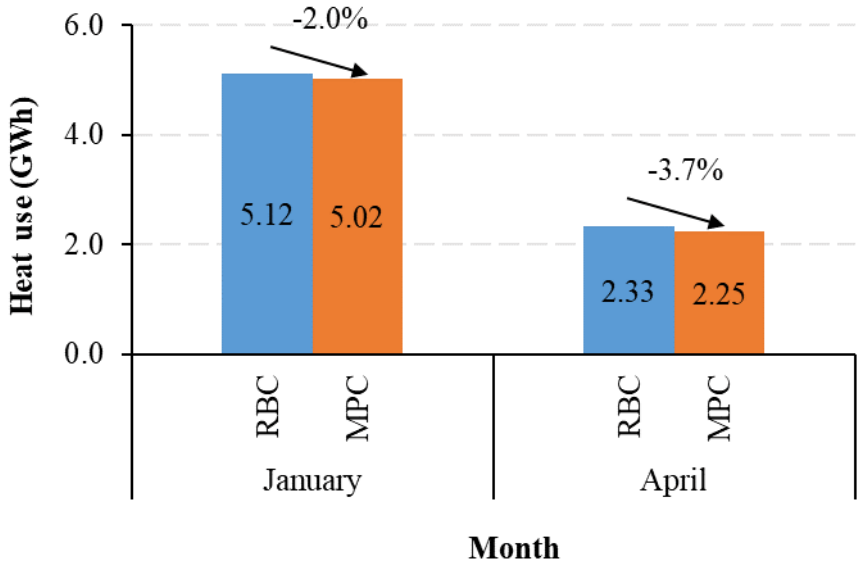

Fig. 13. Simulated heat use for two scenarios

4.4. Overall performance of heat prosumer

The total energy use and energy bill were used to evaluate the heat prosumer's overall performance. Fig. 14 presents the monthly total energy use for the two scenarios. The energy use included the heat supplied from the MS and the electricity supplied to power the DC's HP and the CP. One obvious result that can be noticed from Fig. 14 was that both the MPC scenarios preferred

to use more electricity but less heat. In January, the heat supplied from the MS for the MPC scenario was 5.02 GWh, a decrease of 2.0% compared to the RBC scenario. In contrast, more electricity was used in the MPC scenario, with an increase of 8.1%. A similar phenomenon could be found in April as well: the heat use decrease was 3.7% and the electricity use increase was almost 19.0% in the MPC scenario. This result can be explained by the following reason: the MPC scenarios tended to gain heat as much as possible from the HP of DC to achieve the maximum economic performance, because the COPs of HP were always higher than 1.0 and maintained at around 3.0-3.1. For example, to supply 3.0 kWh of heat for the heat user, the electricity use of HP would be only around 1.0 kWh while the MS would need to supply exactly 3.0 kWh heat. Meanwhile, the prices of electricity were only a bit higher than the heat during the studied period. Therefore, gaining heat as much as possible from the HP was the way that the MPC scheme used to achieve the maximum possible economic performance, and this will be further illustrated in the following text.

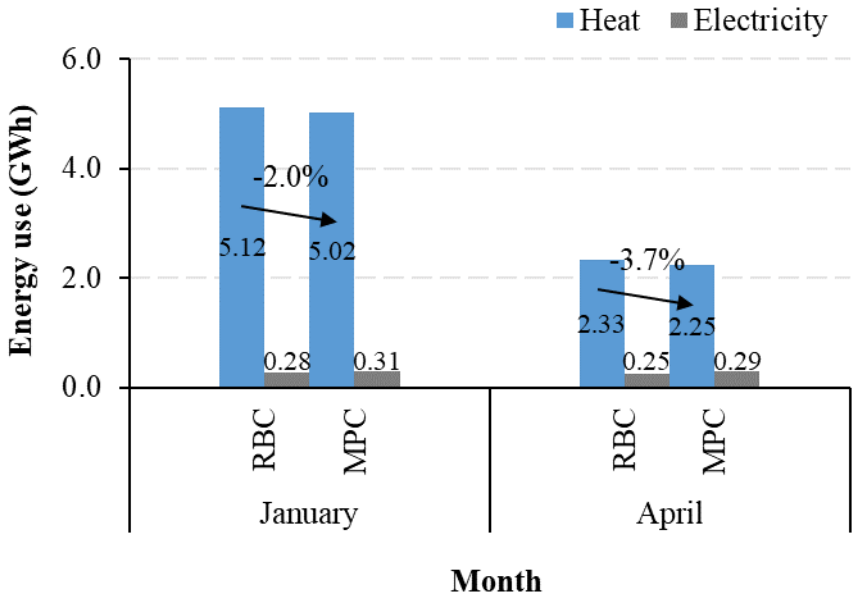

Fig. 14. Simulated energy use for two scenarios

Fig. 15 presents the monthly total energy bill for the two scenarios. The energy bill consisted of heating cost and electricity cost as illustrated in Section 2.2. Thereof, the heating cost included the LDC based on the heat user's peak load and the EDC based on the total heat use of the heat user. There were several similar results presented both in January and April as follows: 1) Both the MPC scenarios saved the total energy bill compared to their corresponding RBC scenarios, with savings of 1.8% and 3.2% in January and April, respectively; 2) Both the MPC scenarios reduced the heating

costs, which were brought by both the reductions of the LDC and the EDC, with the reduction of 2.3% and 5.1% in January and April; 3) Both the MPC scenarios increased the electricity cost due to the increased electricity use as explained by Fig. 14. The increases were 8.2% and 19.1% in January and April, respectively. However, the electricity cost accounted for less than 10% of the total energy bill and hence the increased electricity cost was not able to impair the total economic performance of MPC scenarios. Based on the above analysis, one important result was found as follows: the MPC scheme made an optimized trade-off between the heat use and the electricity use to achieve the possible maximum economic performance of the heat prosumer.

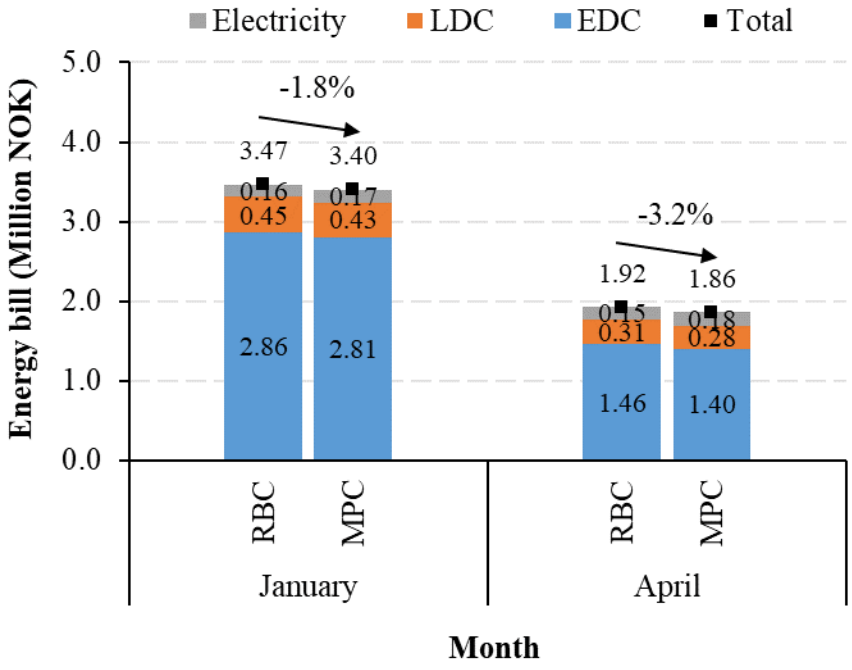

Fig. 15. Simulated energy bill for two scenarios

5. Discussion

In this study, numerous manipulated variables needed to be optimized originating from the multi-components, which increased the computation load of MPC. To tackle this issue, a compromise between the developed model's accuracy and computational tractability should be made. The developed model must be accurate enough to predict the future behaviour of the system, meanwhile, it should be as simple as possible to be computationally tractable and numerically stable [57]. Therefore, the developed HP model in DC was a simplified linear model instead of a second-order model suggested by the ASHRAE handbook [45, 58]. Firstly, the second-order model features

nonlinearity, further increasing the already computing-demanding burden of the MPC scheme. Secondly, the developed linear HP model demonstrated even better prediction performance (R^2 is 0.93) than the second-order model (R^2 is 0.87), as shown in Section Appendix E. As a result, the linear HP model was used for the MPC scheme in this study. In addition, to acquire computing efficiency, one crucial assumption was made: the boundary of the water temperature difference, which was obtained by measured data, at the primary side of the building substation could represent the whole thermal transfer potential of these substations. This assumption may underestimate these potentials if the system is under inappropriate operation, such as the so-called "big flow rate and small temperature difference" operation modes. However, the assumption provided a straightforward method to gain insights into the demand side from easily obtained measurements.

Moreover, different energy price strategies affect the optimal control decisions and hence the system's economic performance. Therefore, a sensitivity analysis of the impact of different energy price strategies on system performance will be conducted in future work.

6. Conclusion

This study aimed to investigate the optimal control of the DC waste heat-based heat prosumer with short-term TES by utilizing an MPC scheme. In this MPC scheme, an economic-related objective function was employed, and both economic boundary and technical operational constraints were formulated. The economic boundary was proposed by considering the heating and electricity pricing mechanism simultaneously, and the technical operational constraints were defined by using the real measured data of the case system. The incorporated model described system dynamics including DC waste heat recovery units, TES, and the local DH system. The proposed MPC scheme was tested by simulation on a campus DH system in Norway. The proposed MPC scheme together with a conventional RBC strategy was evaluated in terms of the DC performance, the local DH system performance, and the overall performance of the heat prosumer.

Results showed that the MPC scheme was more stable and robust expressed as the smaller fluctuating ranges of both the outlet temperature of the evaporator and the COP of the HP in DC, which are crucial for the DC cooling system's safe operation. In addition, the MPC scheme took better advantage of the WTTES flexibilities, which was demonstrated by the lower peak loads. The peak load reduction of the MPC scheme was up to 12.0% compared to the RBC strategy. Finally, the MPC

scheme tended to gain waste heat as much as possible from the DC by using more electricity for the HP but extracting less heat from the MS to achieve the maximum possible economic performance, and the resulting monthly energy cost saving was up to 3.2%. In total, the MPC scheme made an optimized trade-off between heat use and electricity use to achieve the best economic performance of the heat prosumer.

This study may provide guidelines on optimal control of the DH system after integrating DC waste heat, and contribute to the development of the implementation of MPC at a local level.

Acknowledgement

The authors gratefully acknowledge the support from the Research Council of Norway through the research project Understanding behaviour of district heating systems integrating distributed sources under the FRIPRO/FRINATEK program (project number 262707).

Appendix A. Energy and mass flow exchanging between individual components

$$\dot{Q}_{MS}=\dot{Q}_{HE1}+\dot{Q}_{HE2} \quad \text{(A- 1)}$$

$$\dot{Q}_{HE1}+\dot{Q}_{HE2}+\dot{Q}_{DC}=\dot{Q}_{Bui}+\dot{Q}_{WTTES}+\dot{Q}_{loss,\ WTTES}+\dot{Q}_{loss,\ pip} \quad \text{(A- 2)}$$

$$\dot{Q}_{HE1}=c\cdot\dot{m}_{HE1}\cdot(T_{sup,HE1}-T_{ret,HE1}) \quad \text{(A- 3)}$$

$$\dot{Q}_{HE2}=c\cdot\dot{m}_{HE2}\cdot(T_{sup,HE2}-T_{ret,HE2}) \quad \text{(A- 4)}$$

$$\dot{Q}_{DC}=c\cdot\dot{m}_{DC}\cdot(T_{sup,DC}-T_{ret,DC}) \quad \text{(A- 5)}$$

where $\dot{Q}$, $\dot{Q}_{loss}$, $\dot{m}$, T_{sup} and T_{ret} represent the heat flow rate, heat loss flow rate, water mass flow rate, supply water temperature and return water temperature, respectively. Subscripts *MS*, *HE1*, *HE2*, *DC*, *Bui*, *WTTES*, and *pip* denote MS, HE1, HE2, DC, building, WTTES, and pipeline. c is the specific heat capacity of water.

Appendix B. Water tank thermal energy storage model

$$c\cdot\rho\cdot A_{XS}\cdot\frac{\partial T}{\partial t}=c\cdot(\dot{m}_{sou}-\dot{m}_{use})\cdot\frac{\partial T}{\partial x}-U\cdot P\cdot(T(t,x)-T_{amb})+\varepsilon\cdot A_{XS}\cdot\frac{\partial^2 T}{\partial x^2} \quad \text{(A- 6)}$$

where T denotes the water temperature inside WTTES. x, P and A_{XS} represent the perimeter, the cross-sectional area and the height of WTTES. t is the time. ρ is the water density. $\dot{m}_{sou}$ and $\dot{m}_{use}$

denote the water mass flow rate at the heat source and heat user side, respectively. T_{amb} refers to the ambient temperature. U represents the U-value of WTTES wall. ε is a parameter that describes the combined heat transfer effect of water due to turbulent flow via conduction, diffusion, and mixing.

Appendix C. Building model

$$\dot{Q}_{Bui}=c\cdot\dot{m}_{Bui}\cdot(T_{sup,bui}-T_{ret,bui}) \quad \text{(A- 7)}$$

$$\Delta T_{Bui,\,L}\leq\Delta T_{Bui}=T_{sup,bui}-T_{ret,bui}\leq\Delta T_{Bui,U} \quad \text{(A- 8)}$$

$$T_{sup,SH,L}\leq T_{sup,bui}\leq T_{sup,SH,U} \quad \text{(A- 9)}$$

$$\dot{m}_{Bui,\,L}\leq\dot{m}_{Bui}\leq\dot{m}_{Bui,\,U} \quad \text{(A- 10)}$$

where $\dot{m}_{Bui}$, $T_{sup,bui}$, $T_{ret,bui}$, ΔT_{Bui} are the water mass flow rate, the supply and the return water temperature and the water temperature difference of the primary side in building substation. Subscripts L and U denote the lower bound and upper bound, respectively.

Appendix D. Pipeline model

$$\dot{Q}_{loss,\,pip}=\dot{Q}_{loss,\,pip,sup}+\dot{Q}_{loss,\,pip,ret} \quad \text{(A- 11)}$$

$$\dot{Q}_{loss,\,pip,sup}=L\cdot\pi\cdot d\cdot\frac{(R_g+R_i)\cdot\Delta T_{pip,sup}-R_c\cdot\Delta T_{pip,ret}}{(R_g+R_i)^2-R_c^{\,2}} \quad \text{(A- 12)}$$

$$\dot{Q}_{loss,\,pip,ret}=L\cdot\pi\cdot d\cdot\frac{(R_g+R_i)\cdot\Delta T_{pip,ret}-R_c\cdot\Delta T_{pip,sup}}{(R_g+R_i)^2-R_c^{\,2}} \quad \text{(A- 13)}$$

where $\dot{Q}_{loss,\,pip,sup}$ and $\dot{Q}_{loss,\,pip,ret}$ are the supply pipe heat loss and the return pipe heat loss. L and d are the route length and the outer pipe diameter, respectively. R_i, R_g, and R_c denote the heat resistance of insulation, ground, and coinciding, respectively. $\Delta T_{pip,sup}$ and $\Delta T_{pip,ret}$ represent the supply pipe temperature difference and the return pipe temperature difference.

Appendix E. Identified second-order heat pump model

$$\widehat{E}_{HP\_sec}=0.9908+1.1879\cdot(T_{out\_con}-T_{mea\_eva})+0.0401\cdot T_{out\_con}-$$
$$T_{mea\_eva})^2-0.0256\cdot\dot{Q}_{con}+4.7800\times10^{-5}\cdot\dot{Q}_{con}^{\,2}+0.0029\cdot(T_{out\_con}-T_{mea\_eva})\cdot\dot{Q}_{con} \quad \text{(A- 14)}$$
$$(R^2=0.87)$$

where $\widehat{E}_{HP\_sec}$ is the simulated compressor power. T_{mea_eva} is the average water temperature flowing in and out of the evaporator. $\dot{Q}_{con}$ is the heat flow rate on the condenser side, which equals to $\dot{Q}_{DC}$ [45].

References

[1] Werner S. International review of district heating and cooling. Energy. 2017;137:617-31.

[2] Frederiksen S, Werner S. District heating and cooling, Vol. 579, Studentlitteratur Lund, 2013.

[3] Lund H, Østergaard PA, Chang M, Werner S, Svendsen S, Sorknæs P, et al. The status of 4th generation district heating: Research and results. Energy. 2018;164:147-59.

[4] Li H, Nord N. Transition to the 4th generation district heating-possibilities, bottlenecks, and challenges. Energy Procedia. 2018;149:483-98.

[5] Luo Y, Cheng N, Zhang S, Tian Z, Xu G, Yang X, et al. Comprehensive energy, economic, environmental assessment of a building integrated photovoltaic-thermoelectric system with battery storage for net zero energy building. Conference Comprehensive energy, economic, environmental assessment of a building integrated photovoltaic-thermoelectric system with battery storage for net zero energy building. Springer, p. 1-19.

[6] Li H, Hou J, Hong T, Ding Y, Nord N. Energy, economic, and environmental analysis of integration of thermal energy storage into district heating systems using waste heat from data centres. Energy. 2021;219:119582.

[7] Wahlroos M, Pärssinen M, Manner J, Syri S. Utilizing data center waste heat in district heating–Impacts on energy efficiency and prospects for low-temperature district heating networks. Energy. 2017;140:1228-38.

[8] Khosravi A, Laukkanen T, Vuorinen V, Syri S. Waste heat recovery from a data centre and 5G smart poles for low-temperature district heating network. Energy. 2021;218:119468.

[9] Huang P, Copertaro B, Zhang X, Shen J, Löfgren I, Rönnelid M, et al. A review of data centers as prosumers in district energy systems: Renewable energy integration and waste heat reuse for district heating. Applied Energy. 2020;258:114109.

[10] Greenberg S, Mills E, Tschudi B, Rumsey P, Myatt B. Best practices for data centers: Lessons learned from benchmarking 22 data centers. Proceedings of the ACEEE Summer Study on Energy Efficiency in Buildings in Asilomar, CA ACEEE, August. 2006;3:76-87.

[11] Lu T, Lü X, Remes M, Viljanen M. Investigation of air management and energy performance in a data center in Finland: Case study. Energy and Buildings. 2011;43(12):3360-72.
[12] Nadjahi C, Louahlia H, Lemasson S. A review of thermal management and innovative cooling strategies for data center. Sustainable Computing: Informatics and Systems. 2018;19:14-28.
[13] Li J, Yang Z, Li H, Hu S, Duan Y, Yan J. Optimal schemes and benefits of recovering waste heat from data center for district heating by CO2 transcritical heat pumps. Energy Conversion and Management. 2021;245:114591.
[14] Hiltunen P, Syri S. Low-temperature waste heat enabling abandoning coal in Espoo district heating system. Energy. 2021;231:120916.
[15] Davies G, Maidment G, Tozer R. Using data centres for combined heating and cooling: An investigation for London. Applied Thermal Engineering. 2016;94:296-304.
[16] He Z, Ding T, Liu Y, Li Z. Analysis of a district heating system using waste heat in a distributed cooling data center. Applied Thermal Engineering. 2018;141:1131-40.
[17] Wahlroos M, Pärssinen M, Rinne S, Syri S, Manner J. Future views on waste heat utilization–Case of data centers in Northern Europe. Renewable and Sustainable Energy Reviews. 2018;82:1749-64.
[18] Drgoňa J, Arroyo J, Cupeiro Figueroa I, Blum D, Arendt K, Kim D, et al. All you need to know about model predictive control for buildings. Annual Reviews in Control. 2020;50:190-232.
[19] Killian M, Kozek M. Ten questions concerning model predictive control for energy efficient buildings. Building and Environment. 2016;105:403-12.
[20] Afram A, Janabi-Sharifi F. Theory and applications of HVAC control systems - A review of model predictive control (MPC). Building and Environment. 2014;72:343-55.
[21] Saletti C, Gambarotta A, Morini M. Development, analysis and application of a predictive controller to a small-scale district heating system. Applied Thermal Engineering. 2020;165:114558.
[22] Vandermeulen A, van der Heijde B, Helsen L. Controlling district heating and cooling networks to unlock flexibility: A review. Energy. 2018;151:103-15.
[23] Verrilli F, Srinivasan S, Gambino G, Canelli M, Himanka M, Del Vecchio C, et al. Model predictive control-based optimal operations of district heating system with thermal energy storage and flexible loads. IEEE Transactions on Automation Science and Engineering. 2016;14(2):547-57.
[24] Saletti C, Zimmerman N, Morini M, Kyprianidis K, Gambarotta A. Enabling smart control by optimally managing the State of Charge of district heating networks. Applied Energy. 2021;283:116286.

[25] Hermansen R, Smith K, Thorsen JE, Wang J, Zong Y. Model predictive control for a heat booster substation in ultra low temperature district heating systems. Energy. 2022;238:121631.
[26] Lyons B, O'Dwyer E, Shah N. Model reduction for Model Predictive Control of district and communal heating systems within cooperative energy systems. Energy. 2020;197:117178.
[27] Aoun N, Bavière R, Vallée M, Aurousseau A, Sandou G. Modelling and flexible predictive control of buildings space-heating demand in district heating systems. Energy. 2019;188:116042.
[28] Leitner B, Widl E, Gawlik W, Hofmann R. Control assessment in coupled local district heating and electrical distribution grids: Model predictive control of electric booster heaters. Energy. 2020;210:118540.
[29] Li H, Hou J, Hong T, Nord N. Distinguish between the economic optimal and lowest distribution temperatures for heat-prosumer-based district heating systems with short-term thermal energy storage. Energy. 2022;248:123601.
[30] Li H, Hou J, Tian Z, Hong T, Nord N, Rohde D. Optimize heat prosumers' economic performance under current heating price models by using water tank thermal energy storage. Energy. 2022;239:122103.
[31] Knudsen BR, Rohde D, Kauko H. Thermal energy storage sizing for industrial waste-heat utilization in district heating: A model predictive control approach. Energy. 2021;234:121200.
[32] Nord N, Shakerin M, Tereshchenko T, Verda V, Borchiellini R. Data informed physical models for district heating grids with distributed heat sources to understand thermal and hydraulic aspects. Energy. 2021;222:119965.
[33] Song J, Wallin F, Li H. District heating cost fluctuation caused by price model shift. Applied Energy. 2017;194:715-24.
[34] Norwegian Water Resources and Energy Directorate. Energy Regulatory Authority, https://www.nve.no/reguleringsmyndigheten/kunde/nett/nettleie/?ref=mainmenu; 2021 [Accessed 3 November 2021].
[35] Karlsen SS. Investigation of Grid Rent Business Models as Incentive for Demand-Side Management in Buildings-A case study on fully electric operated houses in Norway. Master thesis: Norwegian University of Science and Technology. 2018.
[36] Statistics Norway. Energy and Manufacturing, https://www.ssb.no/en/energi-og-industri/artikler-og-publikasjoner/twofold-increase-in-electricity-price-for-households; 2021 [Accessed 3 November 2021].
[37] Nord Pool. https://www.nordpoolgroup.com/; 2021 [Accessed 3 November 2021].

[38] Energy Facts Norway. Norway's Energy Supply System, https://energifaktanorge.no/en/utskrift/#toc-2; 2021 [Accessed 3 November 2021].
[39] Tensio. Grid Rental, https://ts.tensio.no/kunde/nettleie-priser-og-avtaler; 2021 [Accessed 3 November 2021].
[40] Atam E, Helsen L. Ground-coupled heat pumps: Part 1–Literature review and research challenges in modeling and optimal control. Renewable and Sustainable Energy Reviews. 2016;54:1653-67.
[41] Jin H. Parameter estimation based models of water source heat pumps: Oklahoma State University, 2002.
[42] Kinab E, Marchio D, Rivière P, Zoughaib A. Reversible heat pump model for seasonal performance optimization. Energy and Buildings. 2010;42(12):2269-80.
[43] Underwood C. Heat pump modelling. Advances in Ground-Source Heat Pump Systems: Elsevier; 2016. p. 387-421.
[44] Shu H-W, Duanmu L, Zhu Y-X, Li X-L. Critical COP value of heat pump unit for energy-saving in the seawater-source heat pump district heating system and the analysis of its impact factors. Harbin Gongye Daxue Xuebao(Journal of Harbin Institute of Technology). 2010;42(12):1995-8.
[45] Shu H, Duanmu L, Shi J, Jia X, Ren Z, Yu H. Field measurement and energy efficiency enhancement potential of a seawater source heat pump district heating system. Energy and Buildings. 2015;105:352-7.
[46] Liu X, Zheng ON, Niu F. A simulation-based study on different control strategies for variable speed pump in distributed ground source heat pump systems. ASHRAE Transactions. 2016;122.
[47] Grundfos. Circulator pump, https://product-selection.grundfos.com/no/products/nbg-nbge/nbg/nbg-100-80-160177-97839346?pumpsystemid=1406357823&tab=variant-sizing-results; 2021 [accessed 15 December 2021].
[48] Li H, Hou J, Hong T, Nord N. Distinguish between the economic optimal and lowest distribution temperatures for heat-prosumer-based district heating systems with short-term thermal energy storage. Energy. 2022:123601.
[49] Åkesson J, Årzén K-E, Gäfvert M, Bergdahl T, Tummescheit H. Modeling and optimization with Optimica and JModelica. org—Languages and tools for solving large-scale dynamic optimization problems. Computers & Chemical Engineering. 2010;34(11):1737-49.

[50] Hou J, Li H, Nord N, Huang G. Model predictive control under weather forecast uncertainty for HVAC systems in university buildings. Energy and Buildings. 2021:111793.
[51] Hou J, Li H, Nord N. Nonlinear model predictive control for the space heating system of a university building in Norway. Energy. 2022;253:124157.
[52] Guan J, Nord N, Chen S. Energy planning of university campus building complex: Energy usage and coincidental analysis of individual buildings with a case study. Energy and Buildings. 2016;124:99-111.
[53] Statkraft varme at Tronheim. Products and services, https://www.statkraftvarme.no/globalassets/0/statkraft-varme/produkter-og-tjenester/prisark/jan-2021/trondheim-bedrift-uten-volumledd-bt1.pdf; 2021 [accessed 16 December 2021].
[54] NordlysEnergi. Company, https://www.nordlysenergi.com/bedrift; 2021 [accessed 16 December 2021].
[55] Ahmad T, Chen H, Shair J. Water source heat pump energy demand prognosticate using disparate data-mining based approaches. Energy. 2018;152:788-803.
[56] Wang J, Li G, Chen H, Liu J, Guo Y, Sun S, et al. Energy consumption prediction for water-source heat pump system using pattern recognition-based algorithms. Applied Thermal Engineering. 2018;136:755-66.
[57] Cígler J, Gyalistras D, Široky J, Tiet V, Ferkl L. Beyond theory: the challenge of implementing model predictive control in buildings. Proceedings of 11th Rehva world congress, Clima2013.
[58] ASHRAE, ASHRAE Applications Handbook, ASHRAE, Atlanta, USA, 1999.